

# Assessing the Webb-Pearman-Leuning Formula in Estimating CO<sub>2</sub> Flux at a Tropical Coast

Muhammad Fikri Sigid<sup>1</sup>, Yusri Yusup<sup>1</sup>, Abdulghani Essayah Swesi<sup>1</sup>, Haitem M Almdhun<sup>1</sup>, and Ehsan Jolous Jamshidi<sup>1</sup>

<sup>1</sup>Universiti Sains Malaysia

March 23, 2023

## Abstract

The Webb-Pearman-Leuning (WPL) formula is used to minimize the overestimate CO<sub>2</sub> flux by open-path gas analyzer and eddy covariance methods. However, its effectiveness for tropical coastal waters with high air water vapor content requires investigation. This paper assesses the WPL correction on CO<sub>2</sub> flux measurement over the tropical coastal water using three calculation methods: standard (including WPL and other correction methods), raw, and WPL. The results showed that the standard method yielded CO<sub>2</sub> flux of  $-0.10 \mu\text{mol m}^{-2} \text{s}^{-1}$ , which is 60% lower than the raw. The WPL-CO<sub>2</sub> flux ( $-0.07 \mu\text{mol m}^{-2} \text{s}^{-1}$ ) is also lower than the raw ( $-0.25 \mu\text{mol m}^{-2} \text{s}^{-1}$ ) by  $0.17 \mu\text{mol m}^{-2} \text{s}^{-1}$ . The WPL formula serves its purpose in minimizing the CO<sub>2</sub> flux overestimation but uses caution with the formula as it can change positive-negative flux signs, especially with temperature and water vapor corrections.



## 21 **Abstract**

22

23 The Webb-Pearman-Leuning (WPL) formula is used to minimize the overestimate CO<sub>2</sub> flux  
24 by open-path gas analyzer and eddy covariance methods. However, its effectiveness for tropical  
25 coastal waters with high air water vapor content requires investigation. This paper assesses the  
26 WPL correction on CO<sub>2</sub> flux measurement over the tropical coastal water using three calculation  
27 methods: standard (including WPL and other correction methods), raw, and WPL. The results  
28 showed that the standard method yielded CO<sub>2</sub> flux of  $-0.10 \mu\text{mol m}^{-2} \text{s}^{-1}$ , which is 60% lower than  
29 the raw. The WPL-CO<sub>2</sub> flux ( $-0.07 \mu\text{mol m}^{-2} \text{s}^{-1}$ ) is also lower than the raw ( $-0.25 \mu\text{mol m}^{-2} \text{s}^{-1}$ )  
30 by  $0.17 \mu\text{mol m}^{-2} \text{s}^{-1}$ . The WPL formula serves its purpose in minimizing the CO<sub>2</sub> flux  
31 overestimation but uses caution with the formula as it can change positive-negative flux signs,  
32 especially with temperature and water vapor corrections.

33

## 34 **Plain Language Summary**

35

36 The Webb-Pearman-Leuning (WPL) formula is a method used to correct overestimation of  
37 CO<sub>2</sub> flux when measuring gas and wind patterns in the air. It has been found to work well in some  
38 areas, but we need to investigate how well it works in tropical coastal waters where the air is very  
39 humid. This study looked at how well the WPL formula works in three different ways of  
40 calculating CO<sub>2</sub> flux: the standard way (which uses WPL and other methods), the raw way (which  
41 doesn't use WPL), and the WPL way. The results showed that the standard way gave a CO<sub>2</sub> flux  
42 of  $-0.10 \mu\text{mol m}^{-2} \text{s}^{-1}$ , which is 60% lower than the raw way. The WPL way gave a CO<sub>2</sub> flux of  $-$   
43  $0.07 \mu\text{mol m}^{-2} \text{s}^{-1}$ , which is lower than the raw way by  $0.17 \mu\text{mol m}^{-2} \text{s}^{-1}$ . The WPL formula is  
44 good at correcting overestimation, but we need to be careful when using it, especially when  
45 correcting for temperature and humidity, because it can change whether the CO<sub>2</sub> flux is positive  
46 or negative.

47

## 48 **1. Introduction**

49

50 Carbon dioxide (CO<sub>2</sub>) fluxes can be directly estimated using the eddy covariance (EC)  
51 technique (Burba et al., 2013). The EC method is often used by ecosystem researchers because it

52 has the advantage of quantifying mass (e.g., CO<sub>2</sub>, methane, water, etc.) and energy (sensible and  
53 latent heat) exchanges of expansive areas, such as forests, croplands, and oceans (Chien et al.,  
54 2018; Heimsch et al., 2021; Lokupitiya et al., 2016; Nakai et al., 2008; Tokoro & Kuwae, 2018).

55  
56 The EC method uses the understanding of the behavior of turbulent eddies and utilizes vertical  
57 turbulent exchange principles to calculate the flux using the covariance of the high-frequency  
58 mixing ratio of CO<sub>2</sub> or moisture and the vertical velocity component of the wind (McGowan et al.,  
59 2016; Stull, 1988). High-frequency measurements of wind velocity components are afforded by  
60 sonic anemometers, but the measurement of CO<sub>2</sub> or moisture (H<sub>2</sub>O) mixing ratio requires fast-  
61 response analyzers. The Infrared Gas Analyzers (IRGA) was developed to measure CO<sub>2</sub> or H<sub>2</sub>O  
62 mixing ratios at high frequencies (e.g., 10 or 20 Hz). At high frequencies, the rapid-response  
63 analyzer could capture turbulent exchange and be able to satisfy the EC method requirement (Jones  
64 & Smith, 1977).

65  
66 The first type of IRGA that measure CO<sub>2</sub> flux on the ocean was the open-path gas analyzer,  
67 and research conducted in the last few decades demonstrated the widespread use of the analyzer  
68 in air-sea CO<sub>2</sub> flux studies (Yang et al., 2016). However, previous studies have shown that the use  
69 of open-path gas analyzer can result in the overestimation of the CO<sub>2</sub> flux due to the effects of  
70 water vapor and temperature (Broecker et al., 1986; Edson et al., 2011; Else et al., 2011; Prytherch,  
71 Yelland, Pascal, Moat, Skjelvan, & Srokosz, 2010). To minimize the error in the calculated flux,  
72 the correction method of the Webb-Pearman-Leuning (WPL) was developed. The WPL  
73 formulation was developed to eliminate the effects of air density fluctuations on the molar density  
74 of CO<sub>2</sub> that could occur in the open-path systems (Burba et al., 2008; Miller et al., 2010). Webb et  
75 al. (1980) proposed the correction by using a formula that considers air density generated by water  
76 vapor and latent heat. Variables of temperature, pressure, and molar density were calculated by the  
77 formula to produce the corrected CO<sub>2</sub> flux from the gas analyzer.

78  
79 On top of the WPL correction, other corrections are applied to the raw CO<sub>2</sub> flux estimated: 1)  
80 wind speed measurement offsets and 2) flux spectral corrections. The offset is necessary because  
81 wind speed readings from a sonic anemometer can be inaccurate because of the measurement drift  
82 (LI-COR, 2021). The spectral corrections are applied to compensate underestimation of fluxes: 1)

83 the low-pass filtering correction for flux losses due to turbulence fluctuation dampening, and 2)  
84 the high-pass filtering correction for flux losses caused by long-term turbulent effects due to the  
85 finite averaging time of fluxes (LI-COR, 2021). The procedures of low-pass filtering correction  
86 are utilized to correct flux spectral properties and describe flux attenuations due to the imperfect  
87 instrumental setup (Moncrieff et al., 1997). The process involves estimating the true co-spectra,  
88 determining a low-pass transfer function, and applying the function to the estimated true flux co-  
89 spectrum so that a high-frequency flux attenuation can be obtained. In addition, the high-frequency  
90 spectral correction performs a simple correction formula based on first-order filters and analytical  
91 co-spectra formulation for high-frequency spectral losses and flux co-spectra (Horst, 1997;  
92 Massman, 2000, 2001; Moncrieff et al., 1997).

93  
94 Some researchers reported that the coastal region is a weak carbon source or uptake (Borges  
95 et al., 2005). The net CO<sub>2</sub> flux measured in northwestern Taiwan was  $-1.75 \pm 0.98 \mu\text{mol m}^{-2} \text{s}^{-1}$ ,  
96 with the diurnal flux influenced by local wind speed. Similarly, in Todos Santos Bay, Mexico, the  
97 CO<sub>2</sub> flux was  $-1.32 \pm 8.94 \mu\text{mol m}^{-2} \text{s}^{-1}$  (Gutiérrez-Loza & Ocampo-Torres, 2016). The CO<sub>2</sub> flux  
98 at Bodega Bay, California, was also a weak source, with  $0.39 \pm 1.84 \mu\text{mol m}^{-2} \text{s}^{-1}$  during the  
99 upwelling period and  $0.05 \pm 0.79 \mu\text{mol m}^{-2} \text{s}^{-1}$  during the relaxation period (Ikawa et al., 2013).  
100 Despite their importance, there is still notable uncertainty in how to parameterize these fluxes for  
101 global climate models, and more observations are necessary to gain a better understanding of the  
102 role of coastal seas in the global carbon cycle (Chien et al., 2018; Doney et al., 2009; Gutiérrez-  
103 Loza & Ocampo-Torres, 2016). Additionally, measuring these fluxes using techniques and  
104 corrections is challenging because of the high uncertainties introduced during data processing,  
105 especially for smaller fluxes (Else et al., 2011; Prytherch, Yelland, Pascal, Moat, Skjelvan, & Neill,  
106 2010). Coastal waters can display high variability in CO<sub>2</sub> flux due to various factors, such as water  
107 temperature, salinity, and biological activity (Ikawa et al., 2013). Despite this, wind speed plays a  
108 critical role in controlling the magnitude of air-sea CO<sub>2</sub> exchanges, and low wind speeds can  
109 restrict gas transfer, resulting in reduced CO<sub>2</sub> fluxes in some cases (Aalto et al., 2021). The flux  
110 over the coast is low compared to fluxes on land (He et al., 2015; Zhang et al., 2014), and low  
111 wind speed over the coast can be one of the reasons that limit gas transfer modulation over coastal  
112 waters (Gutiérrez-Loza & Ocampo-Torres, 2016).

113

114 High-accuracy measurements of CO<sub>2</sub> flux on coastal waters is essential in understanding the  
115 global carbon processes and accuracy of future projection studies of carbon sources and  
116 sequestration. So, the application of the WPL correction to CO<sub>2</sub> flux measurements over the coastal  
117 waters must be investigated. Therefore, the objective of this paper is to assess the WPL correction  
118 method on CO<sub>2</sub> flux measurement at a tropical coastal water location.

119

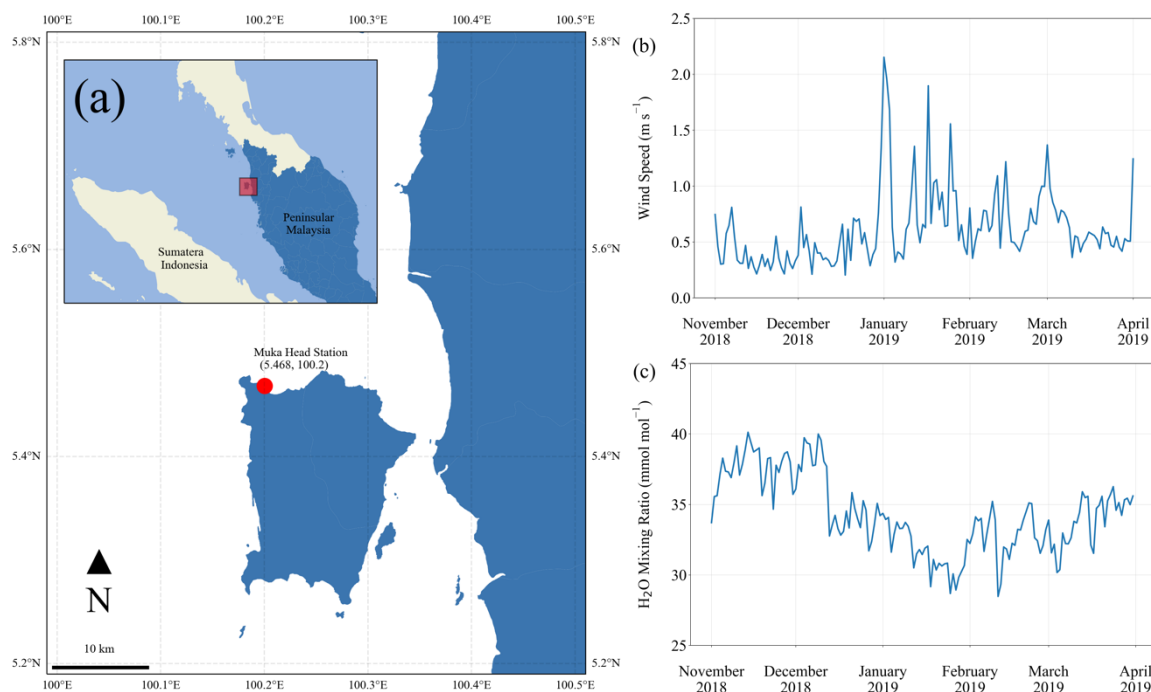
## 120 2. Materials and Methods

121

### 122 2.1 The EC Dataset

123

124 This analysis uses the *in-situ* EC data collected from an automated weather station called the  
125 “Muka Head Station” in the Centre for Marine and Coastal Studies of Universiti Sains Malaysia.  
126 The station is located on the northwestern part of Penang, Peninsular Malaysia at 5°28'06”N,  
127 100°12'01”E (see Figure 1a).



128

129 **Figure 1** (a) Red circle and box show the location of the automated weather station called the  
130 Muka Head Station in Penang, Peninsular Malaysia; (b) the daily-averaged wind speed; (c) the  
131 daily-averaged H<sub>2</sub>O mixing ratio during the Northeast Monsoon.

132 Based on Figure 1b, the range of wind speeds in the study location during the Northeast  
133 Monsoon is between 0.20 m s<sup>-1</sup> and 2.15 m s<sup>-1</sup>, while the average is 0.61 m s<sup>-1</sup>, which is lower  
134 than the coast study area of Gutiérrez-Loza and Ocampo-Torres (2016). Furthermore, the H<sub>2</sub>O  
135 mixing ratio (refer Figure 1c) has an average of 34.31 mmol mol<sup>-1</sup>, with a minimum of 28.47 mmol  
136 mol<sup>-1</sup> and a maximum of 40.12 mmol mol<sup>-1</sup>. Meanwhile, the range of salinity values is relatively  
137 low, with a minimum of 32.74 ‰, a maximum of 34.1 ‰, and an average of 33.43 ‰ since  
138 the site is located over the coast in the tropics, where the salinity is naturally low and does not vary  
139 much (Zhu et al., 2009). Overall, the data suggest that there is a relatively low level of salinity and  
140 wind speeds.

141

142 The station measures CO<sub>2</sub> and H<sub>2</sub>O fluxes and bio-meteorological parameters (global  
143 radiation, net radiation, seawater temperature, etc.) of a tropical coastal ocean in the Strait of  
144 Malacca. The flux is calculated from the 20-Hz data collected by the open-path LI-7500 infrared  
145 CO<sub>2</sub>/H<sub>2</sub>O analyzer (LI-COR, USA) and a sonic anemometer (RM81000, Young, USA). The site  
146 is exposed to minimal anthropogenic influence. Other details of the instrumentation can be seen in  
147 the published literature (Yusup et al., 2020).

148

149 From the entire list of variables available in the dataset, the primary variable analyzed was the  
150 EC's CO<sub>2</sub> flux. The data is accessible at <http://atmosfera.usm.my> and has a time resolution of 30  
151 minutes. The duration of the dataset was from 2015 until 2023, however, the temporal scope of  
152 this analysis is five months. The months sampled are in the Northeast Monsoon (November 2018  
153 – March 2019). Analyses and plots were performed and generated using Python ver. 3.9.

154

## 155 *2.2 Calculations of the Raw, WPL-Corrected, and Standard CO<sub>2</sub> Fluxes*

156

157 The CO<sub>2</sub> flux is calculated “raw” using the EC technique. The method applies the vertical  
158 turbulence exchange concept to calculate the flux directly by using the vertical wind velocity,  
159 molar density of dry air, and the mixing ratio of CO<sub>2</sub> (Aubinet et al., 2000). The EC method uses  
160 Equation (1).

161

$$162 \quad F_{c,raw} = \overline{\rho_a} \overline{w'c'} \quad (1)$$

163  $F_c$  is CO<sub>2</sub> flux,  $\rho_a$  is molar density of dry air,  $w$  is vertical component of wind speed, and  $c$  is dry  
164 air mixing ratio of CO<sub>2</sub>.

165

166 The WPL correction method is applied to the raw CO<sub>2</sub> flux calculated using Equation (1). The  
167 WPL formula is shown in Equation (2).

168

$$169 \quad F_{c,WPL} = \overline{w'\rho'_c} + (1 + \mu\sigma) \frac{\overline{\rho_c}}{\overline{T}} \overline{w'T'} + \mu \frac{\overline{\rho_c}}{\overline{\rho_a}} \overline{w'\rho'_v} + (1 + \mu\sigma) \frac{\overline{\rho_c}}{\overline{P}} \overline{w'P'} \quad (2)$$

170

171  $T$  is temperature,  $P$  is pressure,  $\rho_c$  is molar density of CO<sub>2</sub>,  $\rho_v$  is molar density of water vapor,  $\rho_a$   
172 is molar density of dry air (Webb et al., 1980). Meanwhile,  $\sigma = \rho_v/\rho_a$  and  $\mu = M_a/M_v$  with  $M_a$   
173 is molecular weight of dry air,  $M_v$  is molecular weight of water vapor. The WPL formula consists  
174 of the corrections for temperature, water vapor, and pressure fluctuations in the open-path gas  
175 analyzer, which are stated in the second, third, and fourth terms in the Equation 2. The first term  
176 on the right section of WPL formula is CO<sub>2</sub> flux of EC method that has not been corrected.

177

178 The WPL-corrected CO<sub>2</sub> flux ( $F_{c,WPL}$ ) is compared to the raw CO<sub>2</sub> flux ( $F_{c,raw}$ ) and the  
179 standard-calculated CO<sub>2</sub> flux ( $F_{c,std}$ ).  $F_{c,std}$  is the CO<sub>2</sub> flux that incorporates other corrections in  
180 addition to the WPL correction: 1) wind speed movement offsets, 2) spectral correction of low-  
181 pass filtering and high-pass filtering. The methods used to calculate  $F_{c,std}$  flux are similar to those  
182 utilized in the widely used flux processing software, EddyPro® (ver. 7, LI-COR, USA). In this  
183 research,  $F_{c,std}$  was used to serve as a benchmark to analyze the application of the WPL correction.

184

### 185 2.3 Performance Metrics

186

187 The comparison among the fluxes calculated involves the correlation among the  $F_{c,raw}$ ,  $F_{c,WPL}$ ,  
188 and  $F_{c,std}$ . This analysis used the Pearson correlation coefficient, which determines the degree of  
189 linearity between two quantitative variables and expresses the degree of relationship between  
190 them. The coefficient can be positive or negative, depending on the direction of correspondence  
191 between changes in the two variables.

192

193 In addition, the evaluation metrics of Root Mean Squared Error (RMSE) and Mean Absolute  
194 Error (MAE) were used to measure the magnitude of the error of  $F_{c,raw}$  and  $F_{c,WPL}$  compared to  
195  $F_{c,std}$ . The RMSE takes the square root of the average of squared differences to measure the  
196 average magnitude of the error, while the MAE calculates the average of the absolute differences  
197 between two values to measure the average magnitude of the errors without considering the  
198 direction (positive or negative).

199

### 200 **3. Results and Discussion**

201

#### 202 *3.1 The $F_{c,std}$ Hourly Cycle at the Tropical Coast*

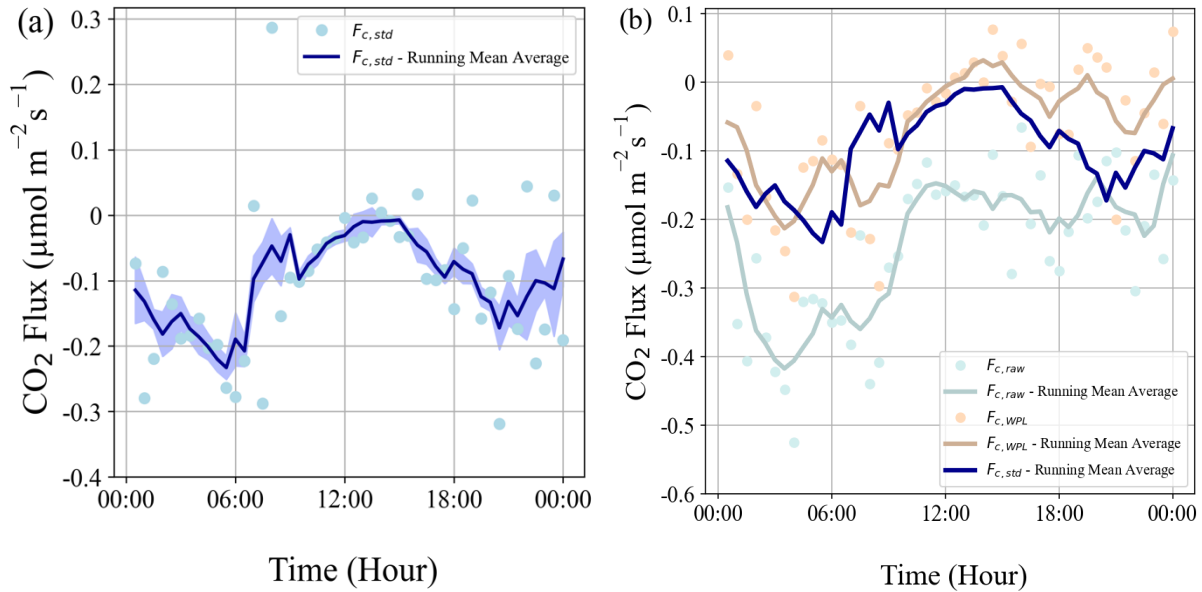
203

204 Throughout the sampling time domain,  $F_{c,std}$  was generally negative, which exhibited that the  
205 tropical coast was a CO<sub>2</sub> sink. It is important to note that the sampling domain is in the Northeast  
206 Monsoon, which is known to be a period of strong upwelling processes (Gayathri et al., 2022;  
207 Mandal et al., 2021; Tan et al., 2006). The magnitude of the negative CO<sub>2</sub> flux varied with the  
208 hours (Figure 2a), but it averaged to  $-0.10 \mu\text{mol m}^{-2} \text{s}^{-1}$ . In the diel cycle, the lowest negative flux  
209 occurred during the daytime, with the flux closing to equilibrium at around 14:00 LT. Meanwhile,  
210 the CO<sub>2</sub> flux during the nighttime displayed greater uptake movements, with the lowest peak  
211 occurring at 06:00 LT.

212

213 This diel cycle is similar to the CO<sub>2</sub> flux trend reported in the Rey–Sánchez et al. (2017) study  
214 as carbon uptake, which was conducted at the coastal waters of the Gulf of Aqaba, Israel. Of note  
215 is the flux magnitude of this site is lower by 90.48% than the cited study's flux ( $-1.05 \mu\text{mol m}^{-2}$   
216  $\text{s}^{-1}$ ). The similarities can be seen in the trend of negative CO<sub>2</sub> fluxes, which reduced towards  
217 equilibrium at 12:00 LT from 06:00 LT; similarly, greater CO<sub>2</sub> uptake occurred during the night.

218



219

220 **Figure 2** (a) The hourly trend of  $F_{c,std}$  and its running-mean average at the tropical coast;

221 (b) the hourly trends of  $F_{c,raw}$ ,  $F_{c,WPL}$ , and  $F_{c,std}$  and their running-mean average.

222

223 Figure 2a also displays the standard error of the  $F_{c,std}$ , indicating a notable level of uncertainty  
 224 during the morning and evening, but a lower level from 09:00 LT until in the afternoon. On  
 225 average, the standard error measures  $0.02 \mu\text{mol m}^{-2} \text{s}^{-1}$ , ranging from a minimum of  $0.005 \mu\text{mol}$   
 226  $\text{m}^{-2} \text{s}^{-1}$  to a maximum of  $0.07 \mu\text{mol m}^{-2} \text{s}^{-1}$ . The observed high uncertainty during specific times  
 227 may be attributed to fluctuations in evaporation. For instance, an increase in the uncertainty to  $0.04$   
 228  $\mu\text{mol m}^{-2} \text{s}^{-1}$  at 08:00 LT was observed due to quite intense fluctuations in evaporation around that  
 229 time, which may have influenced the  $\text{CO}_2$  flux's uncertainty.

230

### 231 3.2 Values and Trends Comparison among the $F_{c,raw}$ , $F_{c,WPL}$ , and $F_{c,std}$

232

233 The average values of  $F_{c,raw}$  and  $F_{c,WPL}$  are  $-0.25$  and  $-0.07 \mu\text{mol m}^{-2} \text{s}^{-1}$ , respectively, and  
 234 both display negative fluxes (refer Figure 2b), which is the same as  $F_{c,std}$ . The decrease of these  
 235 three fluxes typically was observed between 06:00 LT and 12:00 LT. The lower flux magnitudes  
 236 can be attributed to the decrease in wind speed during this period, which lowers the transfer  
 237 velocity and reduces  $\text{CO}_2$  flux in accordance with the bulk formula (Wanninkhof, 1992;  
 238 Wanninkhof et al., 2009).

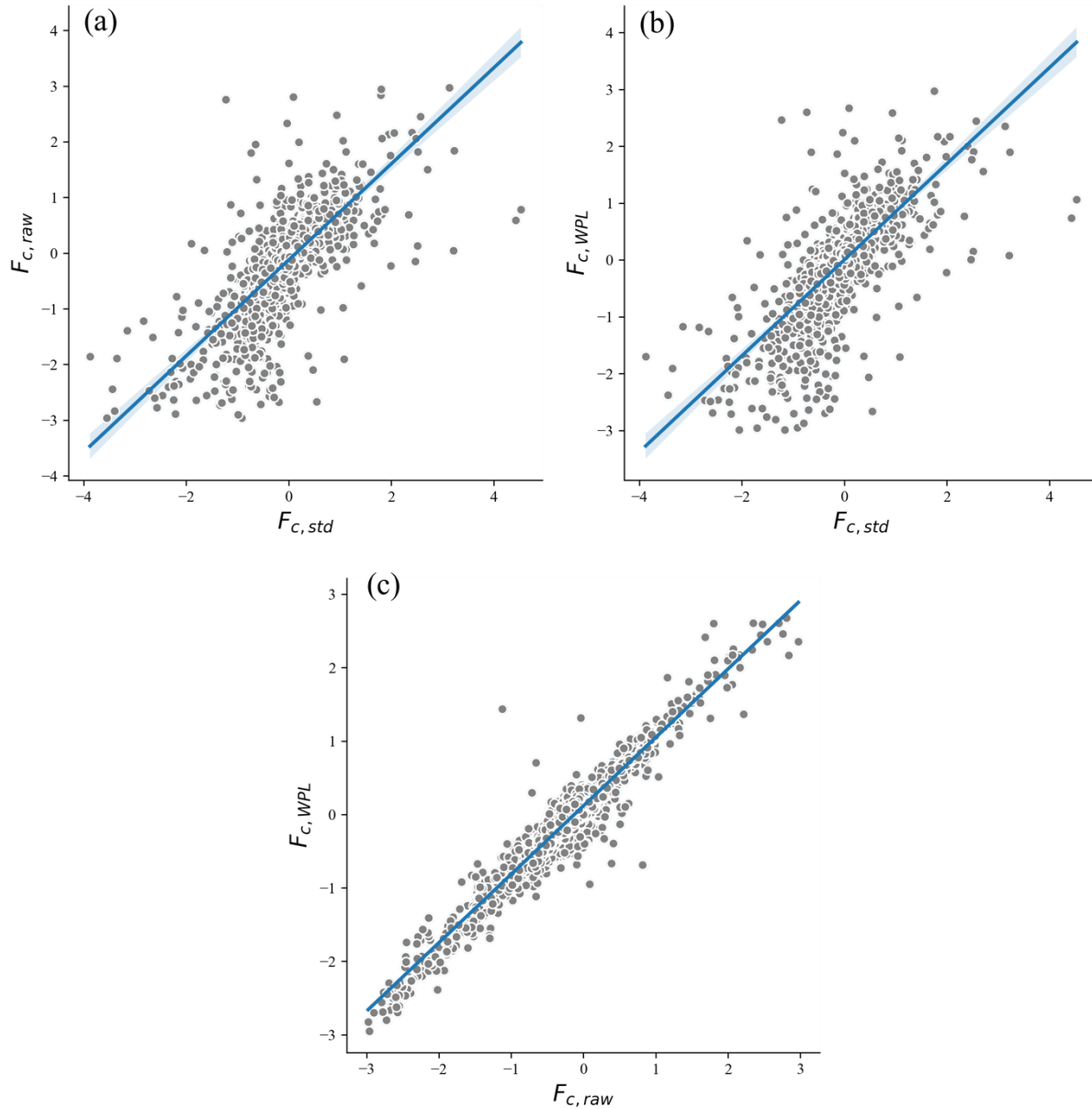
239 There is a varying trend between  $F_{c,raw}$  and  $F_{c,WPL}$  with  $F_{c,std}$ .  $F_{c,raw}$  and  $F_{c,WPL}$  show a  
240 significant increase after 00:00 LT, while  $F_{c,std}$  increases significantly after 12:00 LT, with another  
241 increase occurring from 00:00 LT to 06:00 LT following a decrease before 00:00 LT. The CO<sub>2</sub>  
242 flux diel cycle reported by Rey-Sánchez et al. (2017) is more similar to  $F_{c,raw}$  and  $F_{c,WPL}$  fluxes  
243 than to  $F_{c,std}$ .

244  
245 The average value of  $F_{c,std}$  is significantly lower (higher) than the  $F_{c,raw}$  ( $F_{c,WPL}$ ) by -60%  
246 (+46%). The difference can be due to the application of correction methods in addition to the WPL  
247 correction. According to LI-COR (2021), wind speed measurement offsets and spectral  
248 corrections, such as low-pass and high-pass filtering, are necessary in estimating CO<sub>2</sub> flux. The  
249 absence of these corrections caused the  $F_{c,WPL}$  to be lower, on average magnitude, than the  $F_{c,std}$ .

250  
251 Between  $F_{c,raw}$  and  $F_{c,WPL}$ ,  $F_{c,WPL}$  is lower than  $F_{c,raw}$  by  $0.17 \mu\text{mol m}^{-2} \text{s}^{-1}$ . This result is the  
252 same as the observation on the open sea by Kondo and Tsukamoto (2007), albeit the magnitude  
253 difference in this research is not as significant as theirs. For instance, the magnitude difference by  
254 the WPL correction in the cited study is higher by  $1.40 \mu\text{mol m}^{-2} \text{s}^{-1}$ . The large difference in the  
255 latter study was accompanied by a higher average magnitude of the  $F_{c,raw}$  reaching up to  $1.42$   
256  $\mu\text{mol m}^{-2} \text{s}^{-1}$ , which can be due to the location of their study, i.e., the open sea with strong winds.  
257 On average, the  $F_{c,WPL}$  is much lower than the  $F_{c,raw}$  flux by >70%–98% for both over the sea and  
258 the coastal waters, but it will result in a CO<sub>2</sub> flux value being close to the  $F_{c,std}$  as well as CO<sub>2</sub> flux  
259 calculated using the bulk transfer equation as measured in Kondo and Tsukamoto (2007). Thus,  
260 despite the deviation, the WPL correction still serves its purpose in reducing the overestimation of  
261 CO<sub>2</sub> flux collected by the open-path gas analyzers.

262  
263 The resulting correlations also highlights the difference in CO<sub>2</sub> flux after applying the WPL  
264 correction (see Figure 3). It shows that the correlation of the  $F_{c,std}$  and  $F_{c,raw}$  (refer Figure 3a) as  
265 well as the correlation of the  $F_{c,std}$  and  $F_{c,WPL}$  (refer Figure 3b) are strong and similar. The  
266 correlation between  $F_{c,WPL}$  and  $F_{c,std}$  is slightly lower than the correlation between  $F_{c,raw}$  and  
267  $F_{c,std}$ , i.e., 0.75 and 0.76, respectively. Moreover, the CO<sub>2</sub> flux trend between the  $F_{c,raw}$  and  $F_{c,WPL}$   
268 is somewhat the same with a very strong correlation ( $r = 0.96$ ) as shown in Figure 3c. It must be

269 pointed out that the lower correlation level between  $F_{c,WPL}$  and  $F_{c,std}$  does not indicate that the  
270 WPL correction reduces the accuracy of the CO<sub>2</sub> flux estimation.  
271



272

273

274 **Figure 3** The scatter plots for (a)  $F_{c,raw}$  and  $F_{c,std}$ , (b)  $F_{c,WPL}$  and  $F_{c,std}$ , and (c)  $F_{c,raw}$  and  $F_{c,WPL}$ .

275

276 The RMSE values for  $F_{c,raw}$  and  $F_{c,WPL}$  were found to be  $0.35 \mu\text{mol m}^{-2} \text{s}^{-1}$  and  $0.33 \mu\text{mol}$   
277  $\text{m}^{-2} \text{s}^{-1}$ , respectively, in comparison to  $F_{c,std}$ . This suggests that the WPL correction reduces the  
278 overall error magnitude, resulting in a more accurate estimation of the CO<sub>2</sub> flux. Moreover, the

279 MAE for  $F_{c,WPL}$  ( $0.18 \mu\text{mol m}^{-2} \text{s}^{-1}$ ) is also lower than the MAE for  $F_{c,raw}$  ( $0.20 \mu\text{mol m}^{-2} \text{s}^{-1}$ )  
280 when compared to  $F_{c,std}$ . This implies that the WPL correction not only reduces the overall error  
281 magnitude but also improves the accuracy of the estimated  $\text{CO}_2$  flux.

282

283 Nevertheless, the WPL correction also produced positive  $\text{CO}_2$  flux several times in the  
284 afternoon and the evening, whereas the  $F_{c,raw}$  only showed negative fluxes as shown in Figure 2b.  
285 For instance, a sign change occurred at 13:30 LT with an  $F_{c,raw}$  value of  $-0.16 \mu\text{mol m}^{-2} \text{s}^{-1}$  and  
286 an  $F_{c,WPL}$  value of  $0.03 \mu\text{mol m}^{-2} \text{s}^{-1}$ . At 16:00 LT, there was also a sign change as the  $F_{c,raw}$  value  
287 is  $-0.11 \mu\text{mol m}^{-2} \text{s}^{-1}$  but the  $F_{c,WPL}$  value is  $0.02 \mu\text{mol m}^{-2} \text{s}^{-1}$ . The different results, particularly  
288 in the change of the negative sign to the positive sign of the  $\text{CO}_2$  flux, can drastically change the  
289 conclusion of the carbon exchange in the studied location. Thus, the WPL correction needs to be  
290 implemented conscientiously to achieve a more meaningful  $\text{CO}_2$  flux measurement.

291

### 292 *3.3 Positive-Negative Sign Change of the $\text{CO}_2$ Flux Due to WPL Correction*

293

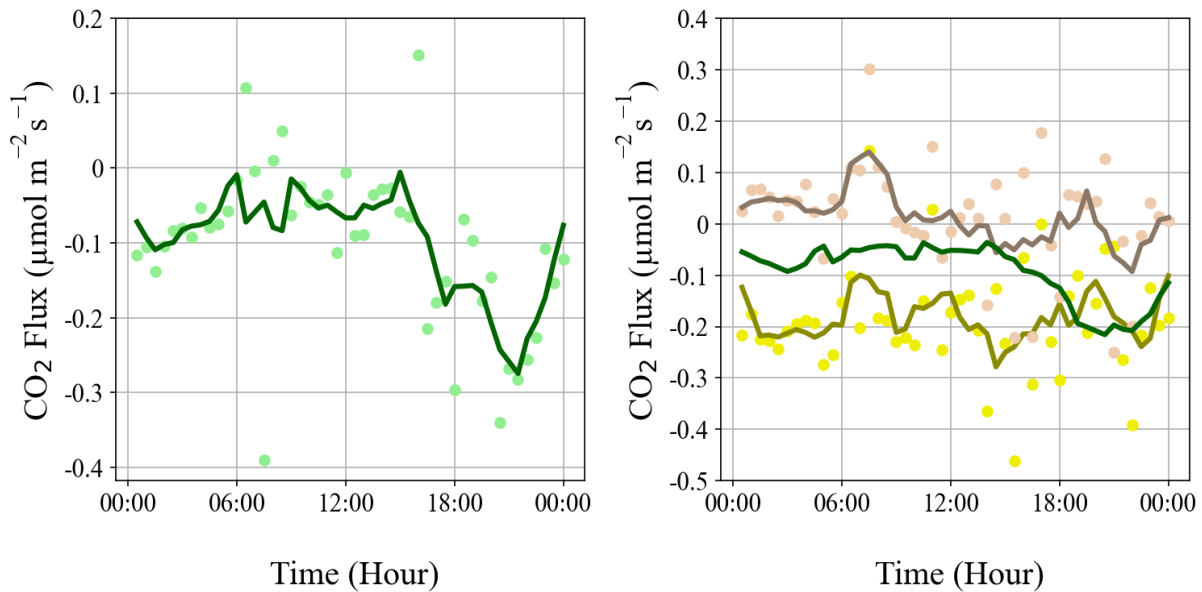
294 Based on  $F_{c,std}$ , the tropical coast acted as  $\text{CO}_2$  uptake, particularly in January 2019. The  $F_{c,std}$   
295 has an average of  $-0.10 \mu\text{mol m}^{-2} \text{s}^{-1}$ , with a similar range of magnitude throughout the Northeast  
296 Monsoon; note that the Northeast Monsoon transpire between November and March, annually.  
297 The magnitude of  $F_{c,std}$  in January also increased in the afternoon, which is the same as the  $F_{c,std}$   
298 in other months in the Northeast Monsoon.

299

300 Compared to the  $\text{CO}_2$  flux diel cycle in the Northeast Monsoon, the flux in January exhibited  
301 a different characteristic than the other months of the monsoon (refer Figure 4). The difference is  
302 apparent in the magnitude of the  $F_{c,std}$  in January; it started to decrease again before 00:00 LT  
303 unlike in other months (see section 3.1). Subsequently, the flux in January fluctuated close to  
304 equilibrium longer until after 15:00 LT. The difference in the characteristics of the  $\text{CO}_2$  flux in  
305 January can be interpreted as the monthly variability of meteorological and oceanographic  
306 parameters that caused different  $\text{CO}_2$  flux responses.

307

308 Based on the CO<sub>2</sub> flux in January (refer Figure 4), the  $F_{c,WPL}$  is also lower than the  $F_{c,raw}$ ,  
 309 confirming the same results of applying the WPL formula in terms of underestimation. The  
 310 absolute average value of the  $F_{c,WPL}$  in this month is lower than the  $F_{c,raw}$  by 93%. Meanwhile,  
 311 the  $F_{c,std}$  is lower than the  $F_{c,raw}$  by 47% but higher than the absolute  $F_{c,WPL}$  by a factor of 75.  
 312 The spectral correction methods of the low-pass and high-pass filtering corrections implemented  
 313 in the  $F_{c,std}$  appears to prevent the underestimation from resulting a sign change of the flux.  
 314



315  
 316 **Figure 4** The hourly trend CO<sub>2</sub> flux for  $F_{c,std}$  (left panel) as well as  $F_{c,raw}$  and  $F_{c,WPL}$  (right  
 317 panel) in January 2019. The yellow, brown, and green colors represent  $F_{c,raw}$  and  $F_{c,WPL}$ , and  
 318  $F_{c,std}$ , respectively. The line is the hourly averaged trend of each  $F_{c,raw}$  and  $F_{c,WPL}$ , and  $F_{c,std}$ .

319  
 320 Between  $F_{c,raw}$  and  $F_{c,WPL}$ , the CO<sub>2</sub> flux calculated using the WPL formula displays a pattern  
 321 that more closely resembled the  $F_{c,std}$ . The  $F_{c,WPL}$  pattern showed a greater magnitude flux during  
 322 evening and lower magnitude flux in the morning until afternoon.

323  
 324 More importantly, the flux underestimation caused by the WPL formula resulted in a changing  
 325 positive-negative sign of the average CO<sub>2</sub> flux. The average for  $F_{c,raw}$  is  $-0.19 \mu\text{mol m}^{-2} \text{s}^{-1}$ ,  
 326 whereas the average for the  $F_{c,WPL}$  flux is  $0.014 \mu\text{mol m}^{-2} \text{s}^{-1}$ . Compared to the Northeast  
 327 Monsoon, the average value of  $F_{c,raw}$  in January is lower, which suggests that the likelihood of a

328 sign change increases when the CO<sub>2</sub> flux is lower or closer to equilibrium. Moreover, Figure 4  
329 shows there are more positive CO<sub>2</sub> flux from 00:00 LT to 12:00 LT for  $F_{c,WPL}$ . Hence, the WPL  
330 correction causes the negative average value of the  $F_{c,raw}$  to change to a positive average value,  
331 which indicate the change in the role of the coast as a source or sink of CO<sub>2</sub>.

332

333 The WPL correction formula indicates that the measurement of  $F_{c,raw}$  is higher in value and  
334 should be corrected for temperature, water vapor, and pressure fluctuations. The largest correction  
335 values are attributed to temperature and water vapor fluctuations, which averaged to  $10^{-6}$  and  $10^{-}$   
336  $^4 \mu\text{mol m}^{-2} \text{ s}^{-1}$ , respectively. In contrast, the correction for pressure fluctuations has the least  
337 significant effect, the difference in average values is a factor of  $10^{300}$ . Consequently, temperature  
338 and water vapor corrections are the most influential factors in altering the sign of CO<sub>2</sub> flux when  
339 applying the WPL correction.

340

#### 341 4 Conclusions

342

343 The WPL formula was introduced to improve the accuracy of CO<sub>2</sub> flux measurement using  
344 the EC method. In this research, the WPL correction was applied on the CO<sub>2</sub> flux measured over  
345 the tropical coastal waters to compare the performance of the correction. Three flux calculation  
346 methods were evaluated: 1) standard (including WPL and other correction methods), 2) raw, and  
347 3) WPL. The  $F_{c,std}$  is lower than  $F_{c,raw}$  by 60% but is higher than  $F_{c,WPL}$  by 46%, which can be  
348 due to additional corrections applied to  $F_{c,std}$ . The  $F_{c,WPL}$  ( $-0.07 \mu\text{mol m}^{-2} \text{ s}^{-1}$ ) is lower than  $F_{c,raw}$   
349 ( $-0.25 \mu\text{mol m}^{-2} \text{ s}^{-1}$ ) by an average of  $0.17 \mu\text{mol m}^{-2} \text{ s}^{-1}$ . The WPL correction and the standard  
350 method produced a clearer hourly CO<sub>2</sub> flux trend than the raw calculated flux. Overall, the WPL  
351 formula produces a lower magnitude flux than the uncorrected CO<sub>2</sub> flux by over 70%, serving its  
352 purpose in minimizing the CO<sub>2</sub> flux overestimation. However, the temperature and water vapor  
353 fluctuations terms in the WPL correction have the greatest impact on altering the positive-negative  
354 sign of CO<sub>2</sub> flux. Therefore, the WPL correction needs to be implemented conscientiously to  
355 obtain a more accurate CO<sub>2</sub> flux using the EC technique over the tropical coast. Further research  
356 is needed to quantify the uncertainty associated with the sign change.

357

358

## 359 Acknowledgements

360

361 We acknowledge that the Malaysian Research University Network Long-Term Research  
362 Grant Scheme (MRUN-LRGS), with grant number 203.PTEKIND.6777006, from the Ministry of  
363 Education Malaysia, enabled us to conduct this research. Additionally, we express our gratitude  
364 towards Elite Scientific Instruments Sdn. Bhd., our industry partner, for their contribution of  
365 sensors that allowed us to take accurate measurements.

366

## 367 Open Research

368

369 The data used in the study was obtained from the Muka Head Station in the Centre for Marine  
370 and Coastal Studies of Universiti Sains Malaysia, it and can be accessed at  
371 <http://atmosfera.usm.my/api.html> (Yusup & Sigid, 2023). The maps used in the study were created  
372 through Cartopy version 0.19.0 (Elson et al., 2021), which is a library for creating maps and  
373 geospatial data visualizations. Cartopy can be accessed at  
374 <https://scitools.org.uk/cartopy/docs/latest/>. The figures were created using Matplotlib version 3.5.1  
375 (Caswell et al., 2021; Hunter, 2007), which is a tool for creating graphs and plots. Matplotlib is  
376 available under the Matplotlib license at <https://matplotlib.org/>.

377

## 378 References

379

- 380 Aalto, N. J., Campbell, K., Eilertsen, H. C., & Bernstein, H. C. (2021). Drivers of Atmosphere-  
381 Ocean CO<sub>2</sub> Flux in Northern Norwegian Fjords. *Frontiers in Marine Science*, 8.  
382 <https://doi.org/10.3389/fmars.2021.692093>
- 383 Aubinet, M., Grelle, A., Ibrom, A., Rannik, Ü., Moncrieff, J., Foken, T., Kowalski, A. S., Martin,  
384 P. H., Berbigier, P., Bernhofer, Ch., Clement, R., Elbers, J., Granier, A., Grünwald, T.,  
385 Morgenstern, K., Pilegaard, K., Rebmann, C., Snijders, W., Valentini, R., & Vesala, T.  
386 (2000). *Estimates of the Annual Net Carbon and Water Exchange of Forests: The*  
387 *EUROFLUX Methodology*.

388 Borges, A. v., Delille, B., & Frankignoulle, M. (2005). Budgeting sinks and sources of CO<sub>2</sub> in the  
389 coastal ocean: Diversity of ecosystem counts. *Geophysical Research Letters*, 32(14), 1–4.  
390 <https://doi.org/10.1029/2005GL023053>

391 Broecker, W. S., Ledwell, J. R., Takahashi, T., Weiss, R., Merlivat, L., Memery, L., Peng, T.-H.,  
392 Jahne, B., & Munnich, K. O. (1986). Isotopic versus micrometeorologic ocean CO<sub>2</sub> fluxes:  
393 A serious conflict. *Journal of Geophysical Research*, 91(C9), 10517.  
394 <https://doi.org/10.1029/jc091ic09p10517>

395 Burba, G., Madsen, R., & Feese, K. (2013). Eddy covariance method for CO<sub>2</sub> emission  
396 measurements in CCUS applications: Principles, instrumentation and software. *Energy*  
397 *Procedia*, 40, 329–336. <https://doi.org/10.1016/j.egypro.2013.08.038>

398 Caswell, T. A., Droettboom, M., Lee, A., Sales De Andrade, E., Hoffmann, T., Hunter, J., Klymak,  
399 J., Firing, E., Stansby, D., Varoquaux, N., Hedegaard Nielsen, J., Root, B., May, R., Elson,  
400 P., Seppänen, J. K., Dale, D., Lee, J.-J., McDougall, D., Straw, A., ... Ivanov, P. (2021).  
401 *matplotlib/matplotlib: REL: v3.5.1*. Zenodo. <https://doi.org/10.5281/zenodo.5773480>

402 Chien, H., Zhong, Y. Z., Yang, K. H., & Cheng, H. Y. (2018). Diurnal variability of CO<sub>2</sub> flux at  
403 coastal zone of Taiwan based on eddy covariance observation. *Continental Shelf Research*,  
404 162, 27–38. <https://doi.org/10.1016/j.csr.2018.04.006>

405 Doney, S. C., Tilbrook, B., Roy, S., Metzl, N., le Quéré, C., Hood, M., Feely, R. A., & Bakker, D.  
406 (2009). Surface-ocean CO<sub>2</sub> variability and vulnerability. *Deep-Sea Research Part II: Topical*  
407 *Studies in Oceanography*, 56(8–10), 504–511. <https://doi.org/10.1016/j.dsr2.2008.12.016>

408 Edson, J. B., Fairall, C. W., Bariteau, L., Zappa, C. J., Cifuentes-Lorenzen, A., McGillis, W. R.,  
409 Pezoa, S., Hare, J. E., & Helmig, D. (2011). Direct covariance measurement of CO<sub>2</sub> gas  
410 transfer velocity during the 2008 Southern Ocean Gas Exchange Experiment: Wind speed  
411 dependency. *Journal of Geophysical Research: Oceans*, 116(11).  
412 <https://doi.org/10.1029/2011JC007022>

413 Else, B. G. T., Papakyriakou, T. N., Galley, R. J., Drennan, W. M., Miller, L. A., & Thomas, H.  
414 (2011). Wintertime CO<sub>2</sub> fluxes in an Arctic polynya using eddy covariance: Evidence for  
415 enhanced air-sea gas transfer during ice formation. *Journal of Geophysical Research:*  
416 *Oceans*, 116(9). <https://doi.org/10.1029/2010JC006760>

417 Elson, P., de Andrade, E. S., Hattersley, R., May, R., Lucas, G., Campbell, E., Dawson, A.,  
418 Raynaud, S., scmc72, Little, B., Donkers, K., Blay, B., Killick, P., Wilson, N., Peglar, P.,

419 lbdreyer, Andrew, Szymaniak, J., Berchet, A., ... Bindle, L. (2021). *SciTools/cartopy:*  
420 *v0.19.0*. Zenodo. <https://doi.org/10.5281/zenodo.4707961>

421 Gayathri, N. M., Sijinkumar, A. v, Nath, B. N., Sandeep, K., & Wei, K. Y. (2022). A ~ 30 kyr sub-  
422 centennial to millennial Indian summer monsoon variability record from the southern  
423 Andaman Sea, northeastern Indian Ocean. *Palaeogeography, Palaeoclimatology,*  
424 *Palaeoecology*, 590, 110865. <https://doi.org/https://doi.org/10.1016/j.palaeo.2022.110865>

425 Gutiérrez-Loza, L., & Ocampo-Torres, F. J. (2016). Air-sea CO<sub>2</sub> fluxes measured by eddy  
426 covariance in a coastal station in Baja California, México. *IOP Conference Series: Earth and*  
427 *Environmental Science*, 35(1). <https://doi.org/10.1088/1755-1315/35/1/012012>

428 He, Y., Yang, J., Zhuang, Q., Harden, J. W., McGuire, A. D., Liu, Y., Wang, G., & Gu, L. (2015).  
429 Incorporating microbial dormancy dynamics into soil decomposition models to improve  
430 quantification of soil carbon dynamics of northern temperate forests. *Journal of Geophysical*  
431 *Research: Biogeosciences*, 120(12), 2596–2611. <https://doi.org/10.1002/2015JG003130>

432 Heimsch, L., Lohila, A., Tuovinen, J. P., Vekuri, H., Heinonsalo, J., Nevalainen, O., Korkiakoski,  
433 M., Liski, J., Laurila, T., & Kulmala, L. (2021). Carbon dioxide fluxes and carbon balance of  
434 an agricultural grassland in southern Finland. *Biogeosciences*, 18(11), 3467–3483.  
435 <https://doi.org/10.5194/bg-18-3467-2021>

436 Horst, T. W. (1997). *A simple formula for attenuation of eddy fluxes measured with first-order-*  
437 *response scalar sensors.*

438 Hunter, J. D. (2007). Matplotlib: A 2D Graphics Environment. *Computing in Science &*  
439 *Engineering*, 9(3), 90–95. <https://doi.org/10.1109/MCSE.2007.55>

440 Ikawa, H., Faloon, I., Kochendorfer, J., Paw U, K. T., & Oechel, W. C. (2013). Air-sea exchange  
441 of CO<sub>2</sub> at a Northern California coastal site along the California Current upwelling system.  
442 *Biogeosciences*, 10(7), 4419–4432. <https://doi.org/10.5194/bg-10-4419-2013>

443 Jones, E. P., & Smith, S. D. (1977). A first measurement of sea-air CO<sub>2</sub> flux by eddy correlation  
444 . *Journal of Geophysical Research*, 82(37), 5990–5992.  
445 <https://doi.org/10.1029/jc082i037p05990>

446 K Webb, B. E., Pearman, G. I., & Leuning, R. (1980). *Correction of flux measurements for density*  
447 *effects due to heat and water vapour transfer* (Vol. 106).

448 Kondo, F., & Tsukamoto, O. (2007). Air-Sea CO<sub>2</sub> Flux by Eddy Covariance Technique in the  
449 Equatorial Indian Ocean. In *Journal of Oceanography* (Vol. 63).

450 LI-COR. (2021). *EddyPro Software Instruction Manual*.

451 Lokupitiya, E., Denning, A. S., Schaefer, K., Ricciuto, D., Anderson, R., Arain, M. A., Baker, I.,  
452 Barr, A. G., Chen, G., Chen, J. M., Ciais, P., Cook, D. R., Dietze, M., el Maayar, M., Fischer,  
453 M., Grant, R., Hollinger, D., Izaurrealde, C., Jain, A., ... Xue, Y. (2016). Carbon and energy  
454 fluxes in cropland ecosystems: a model-data comparison. *Biogeochemistry*, 129(1–2), 53–76.  
455 <https://doi.org/10.1007/s10533-016-0219-3>

456 Mandal, S., Behera, N., Gangopadhyay, A., Susanto, R. D., & Pandey, P. C. (2021). Evidence of  
457 a chlorophyll “tongue” in the Malacca Strait from satellite observations. *Journal of Marine*  
458 *Systems*, 223. <https://doi.org/10.1016/j.jmarsys.2021.103610>

459 Massman, W. J. (2000). A simple method for estimating frequency response corrections for eddy  
460 covariance systems. In *Agricultural and Forest Meteorology* (Vol. 104).

461 Massman, W. J. (2001). Reply to comment by Rannik on “A simple method for estimating  
462 frequency response corrections for eddy covariance systems.” In *Agricultural and Forest*  
463 *Meteorology* (Vol. 107).

464 McGowan, H. A., MacKellar, M. C., & Gray, M. A. (2016). Direct measurements of air-sea CO2  
465 exchange over a coral reef. *Geophysical Research Letters*, 43(9), 4602–4608.  
466 <https://doi.org/10.1002/2016GL068772>

467 Moncrieff, J. B., Massheder, J. M., de Bruin, H., Elbers, J., Friborg, T., Heusinkveld, B., Kabat,  
468 P., Scott, S., Soegaard, H., & Verhoef, A. (1997). A system to measure surface fluxes of  
469 momentum, sensible heat, water vapour and carbon dioxide. In *Journal of Hydrology*  
470 *ELSEVIER Journal of Hydrology*.

471 Nakai, Y., Matsuura, Y., Kajimoto, T., Abaimov, A. P., Yamamoto, S., & Zyryanova, O. A.  
472 (2008). Eddy covariance CO2 flux above a Gmelin larch forest on continuous permafrost in  
473 Central Siberia during a growing season. *Theoretical and Applied Climatology*, 93(3–4), 133–  
474 147. <https://doi.org/10.1007/s00704-007-0337-x>

475 Prytherch, J., Yelland, M. J., Pascal, R. W., Moat, B. I., Skjelvan, I., & Neill, C. C. (2010). Direct  
476 measurements of the CO2 flux over the ocean: Development of a novel method. *Geophysical*  
477 *Research Letters*, 37(3). <https://doi.org/10.1029/2009GL041482>

478 Prytherch, J., Yelland, M. J., Pascal, R. W., Moat, B. I., Skjelvan, I., & Srokosz, M. A. (2010).  
479 Open ocean gas transfer velocity derived from long-term direct measurements of the CO2  
480 flux. *Geophysical Research Letters*, 37(23). <https://doi.org/10.1029/2010GL045597>

481 Rey-Sánchez, A. C., Bohrer, G., Morin, T. H., Shlomo, D., Mirfenderesgi, G., Gildor, H., & Genin,  
482 A. (2017). Evaporation and CO<sub>2</sub> fluxes in a coastal reef: an eddy covariance approach.  
483 *Ecosystem Health and Sustainability*, 3(10). <https://doi.org/10.1080/20964129.2017.1392830>

484 Stull, R. B. (1988). *An Introduction to Boundary Layer Meteorology*.  
485 <https://doi.org/10.1007/978-94-009-3027-8>

486 Tan, J. C. H., Peters, D. M., & Kaufman, P. L. (2006). Recent developments in understanding the  
487 pathophysiology of elevated intraocular pressure. *Current Opinion in Ophthalmology*, 17(2),  
488 168–174. <https://doi.org/10.1016/j.csr.2005.09.008>

489 Tokoro, T., & Kuwae, T. (2018). Improved post-processing of eddy-covariance data to quantify  
490 atmosphere-aquatic ecosystem CO<sub>2</sub> Exchanges. *Frontiers in Marine Science*, 5(AUG).  
491 <https://doi.org/10.3389/fmars.2018.00286>

492 Wanninkhof, R. (1992). Relationship Between Wind Speed and Gas Exchange Over the Ocean. In  
493 *JOURNAL OF GEOPHYSICAL RESEARCH* (Vol. 97, Issue C5).

494 Wanninkhof, R., Asher, W. E., Ho, D. T., Sweeney, C., & McGillis, W. R. (2009). Advances in  
495 quantifying air-sea gas exchange and environmental forcing. In *Annual Review of Marine*  
496 *Science* (Vol. 1, pp. 213–244). <https://doi.org/10.1146/annurev.marine.010908.163742>

497 Webb, E. K., Pearman, G. I., & Leuning, R. (1980). *Correction of flux measurements for density*  
498 *effects due to heat and water vapour transfer* (Vol. 106).

499 Yang, M., Prytherch, J., Kozlova, E., Yelland, M. J., Parenkat Mony, D., & Bell, T. G. (2016).  
500 Comparison of two closed-path cavity-based spectrometers for measuring air-water CO<sub>2</sub> and  
501 CH<sub>4</sub> fluxes by eddy covariance. *Atmospheric Measurement Techniques*, 9(11), 5509–5522.  
502 <https://doi.org/10.5194/amt-9-5509-2016>

503 Yusup, Y., Ramli, N. K., Kayode, J. S., Yin, C. S., Hisham, S., Isa, H. M., & Ahmad, M. I. (2020).  
504 Atmospheric carbon dioxide and electricity production due to lockdown. *Sustainability*  
505 *(Switzerland)*, 12(22), 1–12. <https://doi.org/10.3390/su12229397>

506 Yusup, Y., & Sigid, M. F. (2023). *Assessing the Webb-Pearman-Leuning Formula in Estimating*  
507 *CO<sub>2</sub> Flux at a Tropical Coast*. <https://doi.org/10.6084/m9.figshare.22139939.v1>

508 Zhang, H. F., Chen, B. Z., van der Laan-Luijkx, I. T., Chen, J., Xu, G., Yan, J. W., Zhou, L. X.,  
509 Fukuyama, Y., Tans, P. P., & Peters, W. (2014). Net terrestrial CO<sub>2</sub> exchange over China  
510 during 2001–2010 estimated with an ensemble data assimilation system for atmospheric CO<sub>2</sub>.

511 *Journal of Geophysical Research*, 119(6), 3500–3515.  
512 <https://doi.org/10.1002/2013JD021297>  
513 Zhu, Y., Shang, S., Zhai, W., & Dai, M. (2009). Satellite-derived surface water pCO<sub>2</sub> and air-sea  
514 CO<sub>2</sub> fluxes in the northern South China Sea in summer. *Progress in Natural Science*, 19(6),  
515 775–779. <https://doi.org/10.1016/j.pnsc.2008.09.004>  
516